Heliyon 10 (2024) e25844

Contents lists available at ScienceDirect

Heliyon

journal homepage: www.cell.com/heliyon

Research article

Handheld hyperspectral imaging as a tool for the post-mortem interval estimation of human skeletal remains

Verena-Maria Schmidt [a,1], Philipp Zelger [b,1], Claudia Wöss [a,1], Margot Fodor [c], Theresa Hautz [c], Stefan Schneeberger [c], Christian Wolfgang Huck [d], Rohit Arora [e], Andrea Brunner [f], Bettina Zelger [f], Michael Schirmer [g], Johannes Dominikus Pallua [e,*]

[a] Institute of Forensic Medicine, Medical University of Innsbruck, Muellerstraße 44, 6020 Innsbruck, Austria
[b] University Clinic for Hearing, Voice and Speech Disorders, Medical University of Innsbruck, Anichstrasse 35, 6020 Innsbruck, Austria
[c] OrganLifeTM, Department of Visceral, Transplant and Thoracic Surgery, Medical University of Innsbruck, Innsbruck, Austria
[d] Institute of Analytical Chemistry and Radiochemistry, University of Innsbruck, 6020 Innsbruck, Austria
[e] Department of Orthopaedics and Traumatology, Medical University of Innsbruck, Anichstraße 35, 6020 Innsbruck, Austria
[f] Institute of Pathology, Neuropathology, and Molecular Pathology, Medical University of Innsbruck, Muellerstrasse 44, 6020 Innsbruck, Austria
[g] Department of Internal Medicine, Clinic II, Medical University of Innsbruck, Anichstrasse 35, 6020 Innsbruck, Austria

ARTICLE INFO

Keywords:
Human skeletal remains
Post-mortem interval
Handheld hyperspectral imaging
Digital image analysis
Deep learning

ABSTRACT

In forensic medicine, estimating human skeletal remains' post-mortem interval (PMI) can be challenging. Following death, bones undergo a series of chemical and physical transformations due to their interactions with the surrounding environment. Post-mortem changes have been assessed using various methods, but estimating the PMI of skeletal remains could still be improved. We propose a new methodology with handheld hyperspectral imaging (HSI) system based on the first results from 104 human skeletal remains with PMIs ranging between 1 day and 2000 years. To differentiate between forensic and archaeological bone material, the Convolutional Neural Network analyzed 65.000 distinct diagnostic spectra: the classification accuracy was 0.58, 0.62, 0.73, 0.81, and 0.98 for PMIs of 0 week–2 weeks, 2 weeks–6 months, 6 months–1 year, 1 year–10 years, and >100 years, respectively. In conclusion, HSI can be used in forensic medicine to distinguish bone materials >100 years old from those <10 years old with an accuracy of 98%. The model has adequate predictive performance, and handheld HSI could serve as a novel approach to objectively and accurately determine the PMI of human skeletal remains.

1. Introduction

Accurately determining the post-mortem interval (PMI) of human remains is critical for efficient identification in medico-legal cases. However, estimating the PMI in skeletonized remains after the soft tissue decomposition stage can be challenging. The reliability of such estimations is complex [1,2]. This is mainly due to the complex and varied degradation processes, including

* Corresponding author.
E-mail addresses: verena-maria.schmidt@i-med.ac.at (V.-M. Schmidt), philipp.zelger@tirol-kliniken.at (P. Zelger), claudia.woess@i-med.ac.at (C. Wöss), christian.w.huck@uibk.ac.at (C.W. Huck), rohit.arora@tirol-kliniken.at (R. Arora), andrea.brunner@i-med.ac.at (A. Brunner), bettina.zelger@i-med.ac.at (B. Zelger), schirmer.michael@icloud.com (M. Schirmer), johannes.pallua@i-med.ac.at (J.D. Pallua).
[1] first three authors contributed equally.

https://doi.org/10.1016/j.heliyon.2024.e25844
Received 31 July 2023; Received in revised form 30 January 2024; Accepted 2 February 2024
Available online 3 February 2024

List of abbreviations

CNN	convolutional neural network
CT	computed tomography
HSI	hyperspectral imaging
NIR	near-infrared
PMI	post-mortem interval
LOOCV	leave-one-out cross-validation
ReLU	rectified linear unit
RGB	red-green-blue
ROI	region of interest
THI	tissue haemoglobin index
TWI	tissue water index
VIS	visible

environmental factors such as temperature and humidity and biological factors such as invertebrate and vertebrate scavengers. Other factors that can impact the accuracy of PMI estimation include fluvial transport, bone weathering, disarticulation, scattering, burial, and bone diagenesis [3–15]. Numerous studies have been conducted to estimate human skeletal remains' PMI. However, several methods are costly, require significant time, and are more consistent in estimating PMI for remains with PMIs shorter than five years [3,11,16]. Further research is necessary to improve our understanding of bone decomposition during shorter PMI periods. Currently, most techniques for estimating the PMI of human skeletal remains are designed for remains that have been decomposing for more extended periods (over ten years) or rely on short-term experiments (less than one year post-mortem) involving defleshed bone or partial carcasses. New methods based on controlled experiments are required to enhance our ability to estimate the PMI of human skeletal remains in a state of early decomposition. Since bones interact with their surroundings after death, various chemical and physical processes result [17–19]. Several techniques have been used to estimate the PMI. However, they all have significant flaws in reliability and accuracy [20,21] and are an ongoing challenge in forensic medicine. At present, the following methods have been proposed in addition to the external physical appearance: histopathological surveys [22–24], reactions with mineral acids, reactions with benzidine, nitrogen loss [25], molecular biology [26–31], high-performance liquid chromatography-tandem mass spectrometry [32], metabolomics [33], UV–Vis methods [34–38], radioisotope measurements [39–42], luminol chemiluminescent reactions [40, 43–47], X-ray diffraction [48–50], spectroscopic technology [37,50–63], post-mortem computed tomography (CT) [64], micro-CT [18,50], visible and thermal 3D imaging [65], and entomological methods (succession model, carrion insect development) [66]. All available information from these techniques can be considered the gold standard, but despite the many different methods, the forensic estimation of PMI is still challenging [53].

Objective approaches with new techniques like hyperspectral imaging (HSI) may add information for quicker and more precise PMI calculations. HSI screens for the spatial organization of chemical compounds based on their distinct spectral signatures, like "fingerprints," which extend the spectrometry information into the third dimension [67]. Compositionally unique substances can be recognized and defined by their chemical components by capturing their spectral fingerprints [68–73]. HSI has been widely used in different research areas, starting with geological and botanical studies [74–77] introduced in food industry issues and art conservation and finally expanded into biomedicine [78–87], including intraoperative visualizations used to solve specific intraoperative problem and forensic application [62,88–98].

HSI is based on the physical principles of sensing data from both visible (VIS = 400–650 nm) and near-infrared (NIR = 750–1000 nm) regions of the electromagnetic spectrum. This process has enabled the development of miniaturized HSI devices. Thanks to technological advancements, we have seen the emergence of handheld HSI devices over the past decade, which marks a significant milestone in the practical application of HSI technology. Modern handheld spectrometers could be a valuable addition to traditional methods for PMI research. However, the performance of these new small technologies varies, occasionally with narrower spectrum areas or lesser resolution. Thus, data are required for specific requests. This research aimed to evaluate the appropriateness of a handheld HSI device. The objective is to determine whether these portable HSI devices help to estimate PMI for forensic purposes. The PMI was correlated with the detected properties using handheld HSI measurements and deep learning.

2. Material and methods

2.1. Sample collection and ethical considerations

At the Institute of Forensic Medicine, forensic bone samples (n = 99) – were routinely collected in the course of an autopsy for identifying human skeletal remains by molecular genetic analysis, and archaeological bone samples (n = 5) were collected from European archaeological sites dating back to medieval times. Before handheld HSI measurements, the PMI was mainly classified based on police investigations, including information on the location, time of discovery, environmental conditions and personal items found on the corpses, and the morphological structures of the bones. A few samples were categorized as "some weeks," within the error range, resulting in the samples' assignments in two overlapping classes. When conventional PMI estimations were uncertain, the average

result was used.

Analyses were performed on forensic and archaeological bone samples taken from the diaphysis of the femur. All bones except the archaeological bone materials were equally prepared. A 7-mm-thick half-transversal section was cut from each forensic bone using a handsaw. The periost and bone marrow were removed from the sectional planes. Subsequently, a transverse section was obtained from each archaeological bone using a handsaw. The sections were then air-dried for a few days at room temperature. The time frames used in §57 of the Austrian criminal code were used to determine and adjust the class intervals [99]. Sex estimation was routinely performed using typical anthropological methods such as pelvic bone and skull characteristics [100,101], 101], as well as DNA typing (data not shown). The measured human skeletal remains' anthropological properties and place of discovery are summarized and described in detail in other sources [50,62,102,103]. The 'Staatssammlung für Anthropologie und Paläoanatomie MUC' (SAPM, Munich, Germany) granted permission and provided archaeological bone samples for the study. Additionally, handheld near-infrared (NIR) spectroscopy and micro-computed tomography (CT) were used for all samples [104,105]. Energy dispersive X-ray mapping as wells as reflection-, ATR- and Raman-microscopic imaging was applied to 2 archaeological and 4 forensic bone samples [50,62].

Handheld HSI was used before molecular biological examinations. The measurements were performed under controlled environmental conditions to ensure accuracy and reliability. The experiments were conducted at a stable temperature of 22 °C, and humidity levels were maintained. The room was darkened during the measurements to minimise potential external influences.

The study was conducted after approval by the Ethikkommission der Medizinischen Universität Innsbruck (EK: 1357/2021). Data will be available on request.

2.2. Hyperspectral imaging

Holmer et al. recently described the handheld HSI system in detail [106]. In this study, HSI data was acquired using a contactless and non-ionizing radiation handheld imaging system called TIVITA® Mobile System (Diaspective Vision GmbH, Am Salzhaff, Germany) in reflectance at room temperature (Fig. 1 (A)). All ambient light was switched off to avoid artefacts while acquiring HSI data. The illumination was performed by six integrated halogen spots, which enabled spectral data acquisition in the visible and near-infrared range from 500 to 1000 nm. The effective pixels of the system were 640 x 480 (x-axis, y-axis), and an electro-optical distance measurement system was included for accurate positioning, 50 cm above the sample. The specific wavelength spikes corresponded to biological and molecular conditions at defined tissue spots and depths, and information on the respective tissue could be obtained. Given its contactless and rapid applicability (about 10 s for recording), handheld HSI measurements did not interfere with routine forensic work. Three handheld HSI measurements were performed on each sample (Fig. 1 (B)). Acquired red green blue (RGB), and HSI data were collected and stored for further analysis. Mean spectra were calculated for the 5 PMI classes, and a confusion matrix was generated using a CNN classification method (Fig. 1 (C)). The handheld HSI measurements and data analysis process are presented in Fig. 1.

2.3. Statistical analysis and machine learning

Convolutional Neural Network

A convolutional neural network (CNN) was implemented to analyze and categorize the HSI data. Convolutional networks allow the extraction of non-local features and operations, such as differentiation and summation of the data. In order to achieve that, the kernels of the CNN are trained based on the data at hand. This data corresponds to spectral data with a target data vector indicating a PMI class

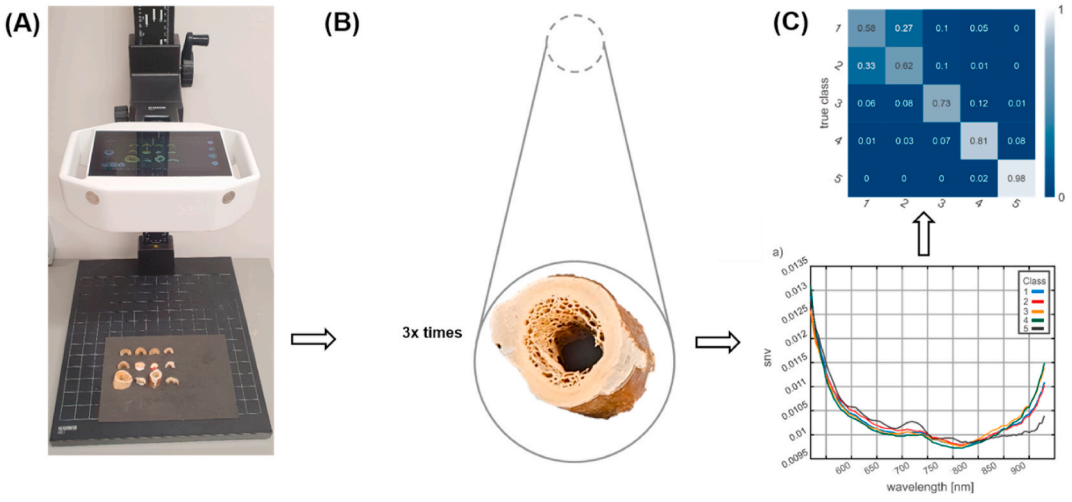

Fig. 1. Handheld HSI measurements and data analysis process. **(A)** Handheld HSI measurement setup. **(B)** Data acquisition process. **(C)** Mean spectra for five different age classes and the confusion matrix of CNN classification.

in the presented case. The network is trained to recognize the members of the individual data sets to the corresponding classes. The present data consists of about 6.000 single spectra per bone sample or 65.000 spectra. The neural network's architecture is based on a ResNet architecture, with three convolutional layers and over 1.500 trainable parameters. The architecture of the neural network is shown in Fig. 2. The network training was performed on an Nvidia GTX 1080 and took 15 min per training. Due to the limited number of samples, a Leave-One-Out Cross-Validation (LOOCV) approach was implemented in training. LOOCV refers to a method where one sample is left out of the training process. In this case, one sample refers to the entirety of all spectra of one bone sample. After the training, the left-out sample is used to evaluate the network. Training a new network from scratch and evaluating its performance on the left-out data set is repeated until every sample has been used as an evaluation sample. A visual representation of the study methodology and CNN architecture is presented in Figs. 2 and 3.

3. Results

The study collected 104 samples from human bones, including 16 from females and 88 from males. The PMIs of the samples were classified into five classes: 0–2 weeks (class 1, n = 32), 2 weeks to 6 months (class 2, n = 46), 6 months to 1 year (class 3, n = 11), 1 year to 10 years (class 4, n = 10), and over 100 years (class 5, n = 5). Prior literature has extensively documented the anthropological characteristics and unearthing of the quantified human skeletal remains [104]. The TIVITA Suite Tissue software provides several images that showcase different physiological parameters of the scanned tissue area. The visual representations utilize a colour gradient to depict the measured quantities, with blue indicating lower values and red indicating higher values. One image shows the tissue's relative blood oxygenation, with an approximate depth of 1 mm. Another image, using the near-infrared (NIR) perfusion index, shows tissue layers at a penetration depth of 4–6 mm. Two additional images display the relative distribution of haemoglobin (Tissue Haemoglobin Index = THI) and water (Tissue Water Index = TWI) in the scanned tissue area, respectively (see Fig. 4) [107,108].

3.1. Convolutional neural network (CNN): prediction of PMI classes

The neural network was trained by feeding with the spectra of the five PMI classes. Fig. 5 shows the mean spectra with standard deviations of all five classes. It is possible to identify the mean of the five sets of spectra displayed in Fig. 5. Nevertheless, it is clear from the standard deviation that the five groups of spectra significantly overlap.

3.2. Classification of the post-mortem interval

HSI is a technique that can provide detailed chemical information about a sample by analyzing its molecular fingerprint and observing various structures or mechanisms related to PMI. Fig. 6a displays the average spectra of five different age categories of PMI, exhibiting class-specific profiles between 500 and 1000 nm. The spectrum showcases distinct peaks at 600 nm, 650 nm, 725 nm and 850 nm.

3.3. Confusion matrix of classification results

In Fig. 6b–a confusion matrix displays how accurately the samples were classified. The diagonal elements correspond to the percentage of correctly classified samples. As per the matrix, the bright diagonal elements represent the percentage of correctly classified samples, which ranges from 98% for archaeological samples (fifth class) to 58% for samples with a PMI between 0 week and 2 weeks (first class). In addition, forensic pathologists estimated the PMI of 13 samples to be "some weeks," due to less information, nine samples had estimated PMIs of "less than 6 weeks." Two samples had estimated PMIs of "less than 10 years." The samples were found in different spots (forest, flat, buried, water) and were subjected to various thermal alterations (plane crash n = 3 and apartment fire n = 1).

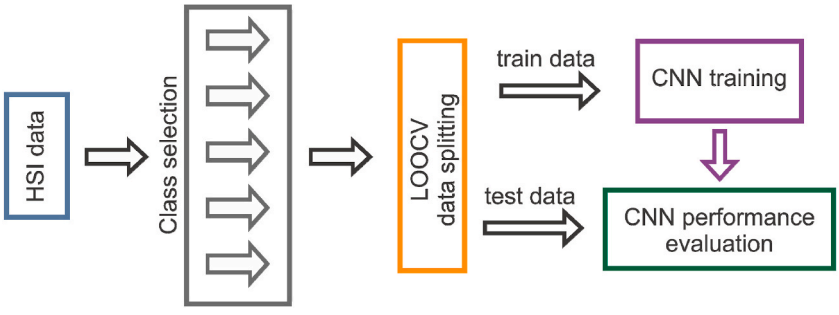

Fig. 2. Schematic representation of the study approach: the procedure was based on extracting handheld HSI information by utilizing a deep learning-based model applying CNN. The data splitting followed the LOOCV approach. I.e., the spectra of one dataset have been used as a test set.

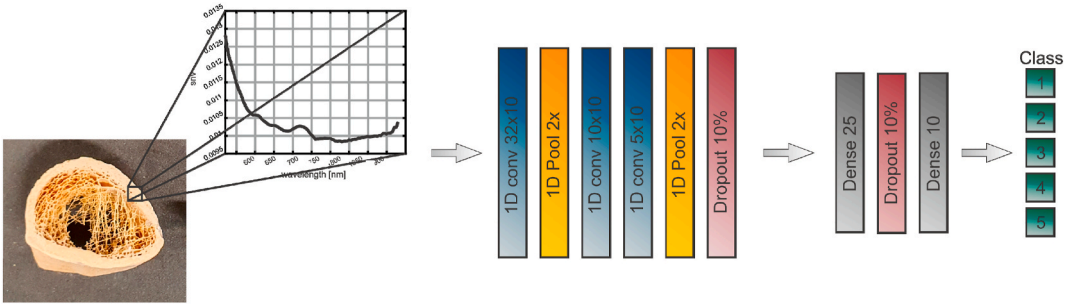

Fig. 3. Schematic representation of the CNN. The network consists of three convolutional (blue) and two dense layers (grey). Both types of layers use a rectified linear unit (ReLU) activation function. Pooling (yellow) and dropout layers (red) have prevented overfitting. The output of the CNN consists of five neurons employing a softmax activation function (green). (For interpretation of the references to color in this figure legend, the reader is referred to the Web version of this article.)

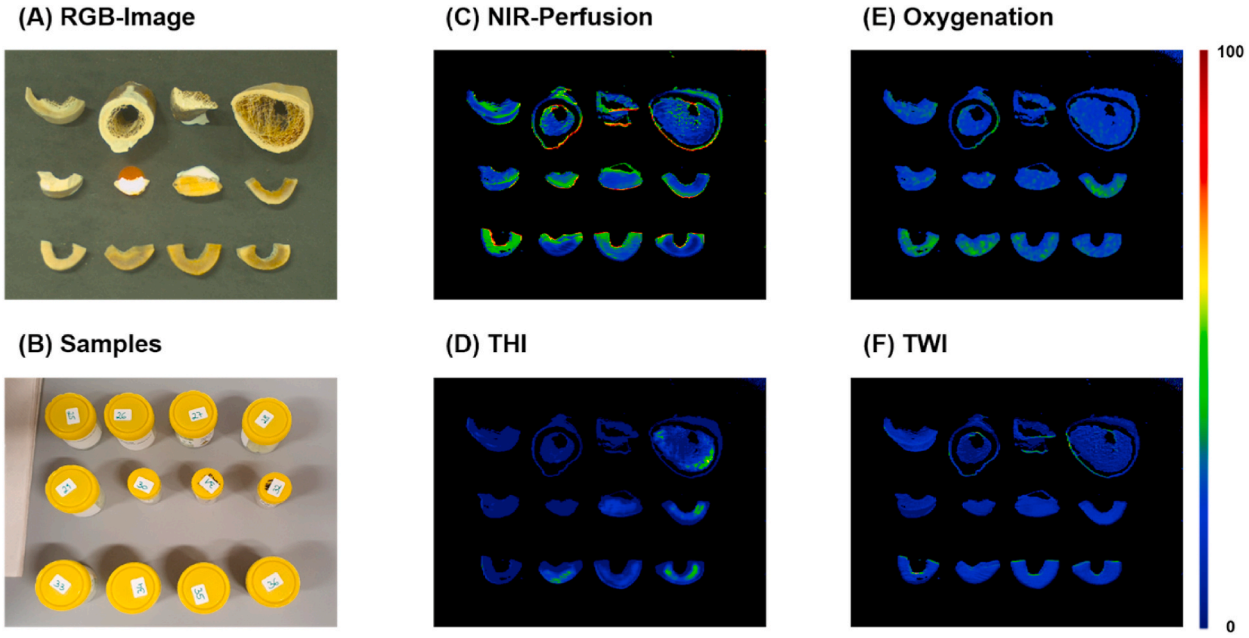

Fig. 4. TIVITA Suite Tissue software results: **(A)** Samples. **(B)** RGB-images. **(C)–(F)** Results for NIR perfusion index (penetration depth of 4–6 mm), the relative distribution of haemoglobin (THI), blood oxigenation and water (TWI) as indicated.

3.4. The Practicability of handheld HSI

HSI is a technique that can be utilized to determine the composition of a sample by measuring the vibrational transitions in its covalent bonds that absorb infrared radiation. This method is rapid and non-contact, and it does not require extensive prior preparation or extraction of samples. With the handheld HSI system and a mobile software application that uses Convolutional Neural Networks (CNN), it is possible to estimate the PMI of human skeletal remains in seconds (Fig. 7).

4. Discussion

The initial findings of a handheld HSI tool for evaluating the PMI in human skeletal remains are presented in this study. Forensic anthropologists and pathologists are keen to develop an accurate technique [56]. A CNN has been effectively trained using a handheld HSI device to predict the PMI of human bones, which will assist authorities in determining whether the bones should be treated as forensic or anthropological samples of interest. Moreover, the classification performance of the CNN can distinguish between forensic and archaeological samples, as Fig. 6b demonstrates variations within the forensic bone sample categories. With 98% accuracy, the fifth class (archaeological samples) is classified ideally, compared to a 58% accuracy in the first class. These findings are new and can provide additional information in estimating PMIs.

The HSI method offers the unique advantage of preserving the sample's integrity before conducting subsequent tests. In

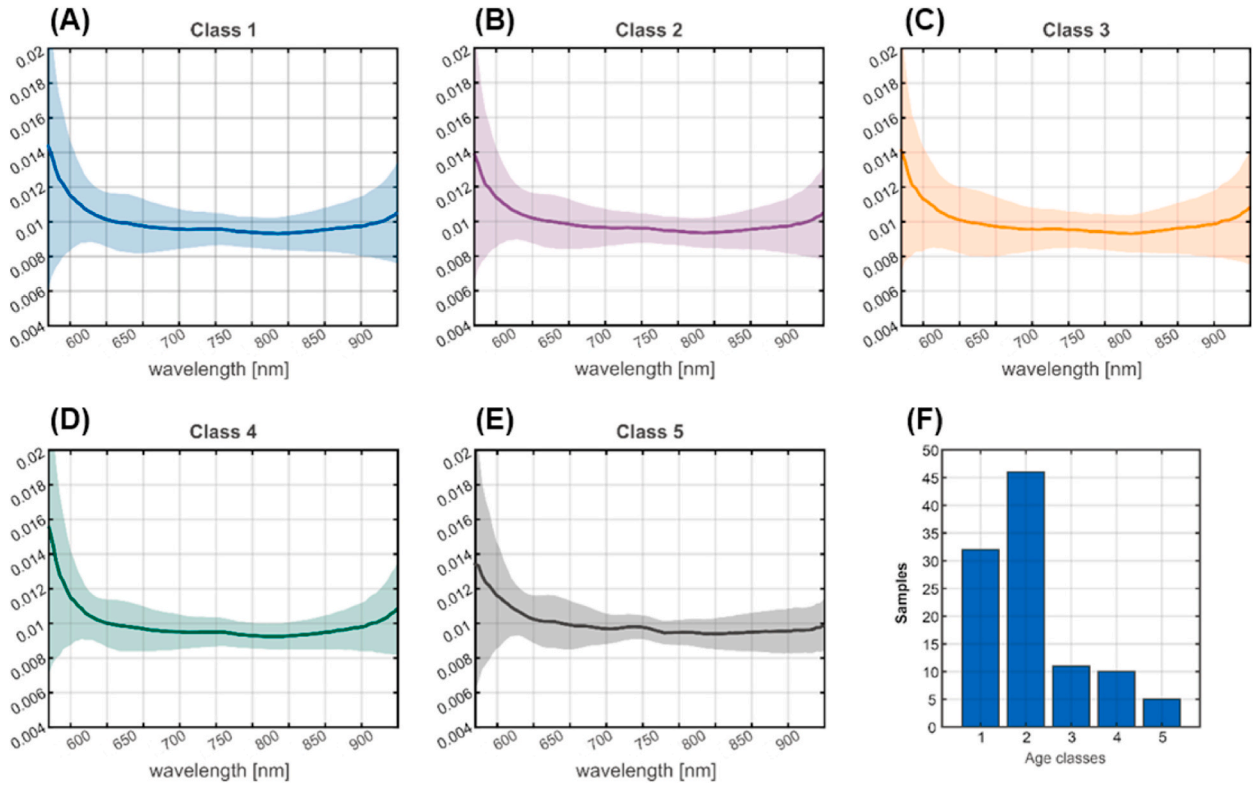

Fig. 5. Mean HSI spectra (colored line) with standard deviations (colored region around the lines) shown for all 5 PMI classes. **(A)** Class 1 (n = 32) ranging between 0 week and 2 weeks. **(B)** Class 2 (n = 46) ranging between 2 weeks and 6 months. **(C)** Class 3 (n = 11) ranging between 6 months and 1 year. **(D)** Class 4 (n = 10) ranging between 1 year and 10 years. **(E)** Class 5 (n = 5) over 100 years. **(F)** Histogram plot shows the number of samples within each class.

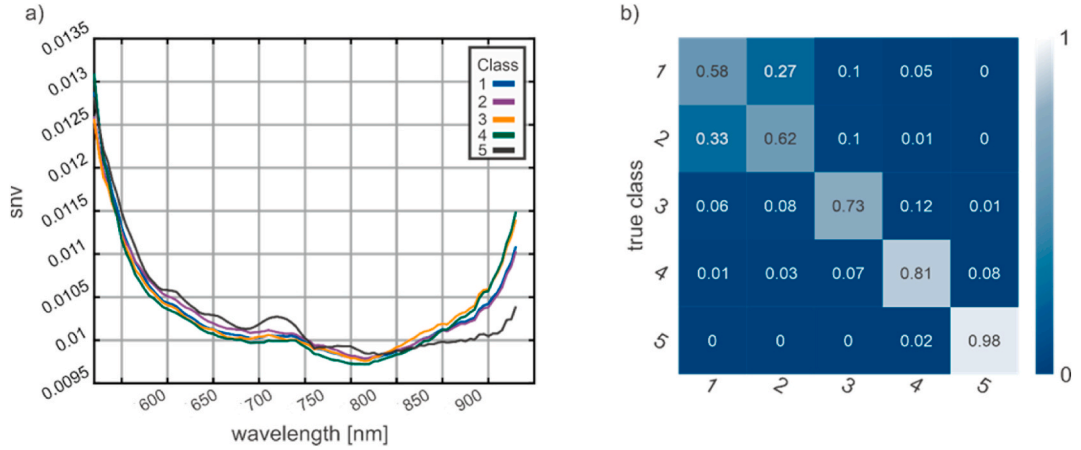

Fig. 6. HSI classification of the PMI: **a)** Mean spectra for five different age classes are represented. Class 1 includes PMI between 0 weeks and 2 weeks (blue line; n = 32), class 2 includes PMI between 2 weeks and 6 months (red line; n = 46), class 3 includes PMI between 6 months and 1 year (orange line; n = 11), class 4 includes PMI between 1 year and 10 years (green line; n = 10), and class 5 includes PMI >100 years (black line; n = 5). **b)** The classification accuracy ranges between 0.58 and 0.98, as per the confusion matrix of CNN classification. (For interpretation of the references to color in this figure legend, the reader is referred to the Web version of this article.)

comparison, most other approaches are more costly and time-consuming [109]. HSI has already been proven to offer valuable diagnostic information for identifying the grades of anaemia and hypoxia, detecting cancer, distinguishing between amalgam tattoos and other dark-pigmented intraoral lesions, and analyzing urinary stones [110–124]. Thus, HSI already provides data for endoscopy [125,126], dermatology [127], macroscopic investigations [128–130], histology [116,117,131–133] and organ viability assessment in

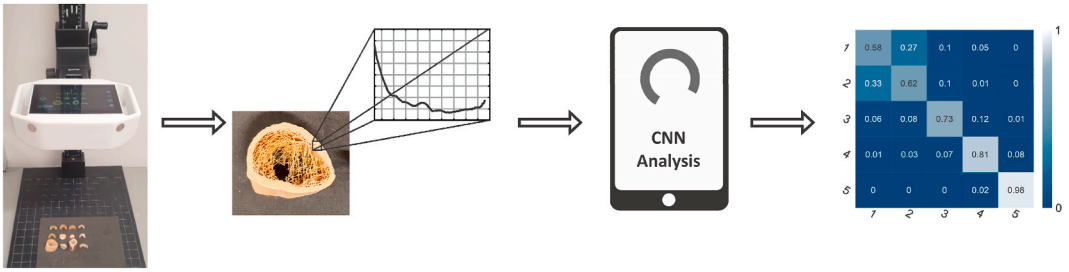

Fig. 7. An analysis workflow for handheld HSI spectra. With high accuracy of almost 98%, the CNN software analyzes the spectra after a single data collection to predict the predicted age class from the input data.

the course of ex-situ machine perfusion [107].

The outcomes of PMI classification are intricate and indicate significant fluctuations in the chemical makeup of bones. Especially the local environment of human skeletal remains triggers particular PMI-related deterioration processes. Thus, HSI results depend on the location of discovery (such as a forest, flat, buried, or body of water), and thermal modifications (apartment fire n = 1 and plane crash n = 3) were also included. Unfortunately, the set of samples is too small to analyze these aspects further. In addition, the premortem bone loss could produce inaccurate findings (as shown, e.g., by earlier CT [105]). More extensive studies are needed to include the locations and prior thermal modifications as independent factors to improve discriminating accuracy between the lower classes 1–4. A combination of non-invasive methods like HSI and CT may solve this problem, but it has not been performed yet.

This HSI study's main limitation is that first-class age uncertainty blurs the distinction between first and second-class [105]. For example, a PMI of 14 days qualifies the sample for the first and second classes. Compared to the age uncertainty in this range (0–7 days), the time window of the first class (0–14 days) amplifies this effect. In samples of the second class with a PMI close to the first class, the same problem occurs. There is a similar effect in all classes except the fifth with PMI of more than 100 years, but not to the same extent. This effect can be explained by the relatively small sample size, with the highest age uncertainty in the first class of PMI lower than 14 days. As the definition of forensic cases widely varies between different countries, with a PMI limited to 15 years in one country and 50 years in another, this study only suggests HSI to distinguish bone materials >100 years from those <10 years with an accuracy of 98%. This limitation could be overcome by a higher number of bone materials with a PMI <10 years.

Another limitation of HSI relates to the chemical composition of bones, depending on the local environment of the skeletal remains. These factors include the discovery location (like forest, flat, buried, or body of water) and thermal modifications. In this study, only a few samples with thermal modifications from incidents like plane crashes and apartment fires further limit the generalizability of the findings. As this is the first study on HSI to determine the PMI of human remains, a sample size calculation was not performed before the study. A more extensive study is warranted to allow a more in-depth analysis of these environmental factors.

Overall, it will be essential to conduct more extensive and multicentric studies with clearly defined PMIs to increase handheld HSI accuracy and improve the performance of the implemented CNN. Comparing these results with NIR spectroscopic analyses, micro-CT of bones, taxonomic identification, preservation processes, diagenetic and thermal alteration pathways, and chemical composition can improve the accuracy of PMI estimation.

5. Conclusions

The handheld HSI tool is an innovative, non-destructive technique that accurately distinguishes between forensic bones and archaeological bone material over 100 years old. This technique is rapid and non-contact, requiring no additional preparation or extraction of samples. By integrating with a mobile software application using Convolutional Neural Networks (CNN), the imaging process takes only a few seconds to complete.

CRediT authorship contribution statement

Verena-Maria Schmidt: Writing – review & editing, Writing – original draft, Investigation, Data curation. **Philipp Zelger:** Writing – review & editing, Writing – original draft, Visualization, Validation, Software, Methodology, Conceptualization. **Claudia Wöss:** Writing – review & editing, Writing – original draft, Validation, Methodology, Investigation, Formal analysis, Data curation, Conceptualization. **Margot Fodor:** Writing – review & editing, Writing – original draft, Methodology, Formal analysis, Data curation. **Theresa Hautz:** Writing – review & editing, Writing – original draft, Resources, Conceptualization. **Stefan Schneeberger:** Writing – review & editing, Writing – original draft, Resources, Conceptualization. **Christian Wolfgang Huck:** Writing – review & editing, Writing – original draft, Resources, Conceptualization. **Rohit Arora:** Writing – review & editing, Writing – original draft, Resources. **Andrea Brunner:** Writing – review & editing, Writing – original draft, Project administration, Conceptualization. **Bettina Zelger:** Writing – review & editing, Writing – original draft, Conceptualization. **Michael Schirmer:** Writing – review & editing, Writing – original draft, Validation, Conceptualization.

Declaration of competing interest

The authors declare that they have no known competing financial interests or personal relationships that could have appeared to influence the work reported in this paper.

Acknowledgements

The authors thank Richard Scheithauer and Walter Rabl for their continuous support. Jan Cemper-Kiesslich from the Institute of Forensic Medicine at the University of Salzburg and Harald Stadler from the University of Innsbruck for providing the medieval bone samples. Additionally, we would like to thank Mario Grubhofer and Nina Neumeister from the Institute of Forensic Medicine at the Medical University of Innsbruck, as well as Clemens Unterwurzacher from the Department of Orthopaedics and Traumatology at the Medical University of Innsbruck for their technical assistance.

References

[1] M.J. Buchan, G.S. Anderson, Time since death: a review of the current Status of methods used in the later postmortem interval, J. Can. Soc. Forensic. Sci. 34 (1) (2001) 1–22.
[2] C. Cattaneo, Forensic anthropology: developments of a classical discipline in the new millennium, Forensic Sci. Int. 165 (2–3) (2007) 185–193.
[3] R.E. Adlam, T. Simmons, The effect of repeated physical disturbance on soft tissue decomposition–are taphonomic studies an accurate reflection of decomposition? J. Forensic Sci. 52 (5) (2007) 1007–1014.
[4] S. Aturaliya, A. Lukasewycz, Experimental forensic and bioanthropological aspects of soft tissue taphonomy: 1. Factors influencing postmortem tissue desiccation rate, J. Forensic Sci. 44 (5) (1999) 893–896.
[5] A. Galloway, W.H. Birkby, A.M. Jones, T.E. Henry, B.O. Parks, Decay rates of human remains in an arid environment, J. Forensic Sci. 34 (3) (1989) 607–616.
[6] R.W. Mann, W.M. Bass, L. Meadows, Time since death and decomposition of the human body: variables and observations in case and experimental field studies, J. Forensic Sci. 35 (1) (1990) 103–111.
[7] M.S. Micozzi, Experimental study of postmortem change under field conditions: effects of freezing, thawing, and mechanical injury, J. Forensic Sci. 31 (3) (1986) 953–961.
[8] A.H. Ross, S.L. Cunningham, Time-since-death and bone weathering in a tropical environment, Forensic Sci. Int. 204 (1–3) (2011) 126–133.
[9] O.J.F. Brown, J. Field, M. Letnic, Variation in the taphonomic effect of scavengers in semi-arid Australia linked to rainfall and the El Niño Southern Oscillation, Int. J. Osteoarchaeol. 16 (2) (2006) 165–176.
[10] R.C. O'Brien, S.L. Forbes, J. Meyer, I.R. Dadour, A preliminary investigation into the scavenging activity on pig carcasses in Western Australia, Forensic Sci. Med. Pathol. 3 (3) (2007) 194–199.
[11] C.M. Fitzgerald, M. Oxenham, Modelling time-since-death in Australian temperate conditions, Aust. J. Forensic Sci. 41 (1) (2009) 27–41.
[12] O.A. Shalaby, L.M. deCarvalho, M.L. Goff, Comparison of patterns of decomposition in a hanging carcass and a carcass in contact with soil in a xerophytic habitat on the Island of Oahu, Hawaii, J. Forensic Sci. 45 (6) (2000) 1267–1273.
[13] B.S. Shean, L. Messinger, M. Papworth, Observations of differential decomposition on sun exposed v. shaded pig carrion in coastal Washington State, J. Forensic Sci. 38 (4) (1993) 938–949.
[14] B. Turner, P. Wiltshire, Experimental validation of forensic evidence: a study of the decomposition of buried pigs in a heavy clay soil, Forensic Sci. Int. 101 (2) (1999) 113–122.
[15] A.S. Wilson, R.C. Janaway, A.D. Holland, H.I. Dodson, E. Baran, A.M. Pollard, D.J. Tobin, Modelling the buried human body environment in upland climes using three contrasting field sites, Forensic Sci. Int. 169 (1) (2007) 6–18.
[16] C.M. Pakosh, T.L. Rogers, Soft tissue decomposition of submerged, dismembered pig limbs enclosed in plastic bags, J. Forensic Sci. 54 (6) (2009) 1223–1228.
[17] M. Vavpotic, T. Turk, D.S. Martincic, J. Balazic, Characteristics of the number of odontoblasts in human dental pulp post-mortem, Forensic Sci. Int. 193 (1–3) (2009) 122–126.
[18] N. Akbulut, S. Cetin, B. Bilecenoglu, A. Altan, S. Akbulut, M. Ocak, K. Orhan, The micro-CT evaluation of enamel-cement thickness, abrasion, and mineral density in teeth in the postmortem interval (PMI): new parameters for the determination of PMI, Int. J. Leg. Med. 134 (2) (2020) 645–653.
[19] B. Madea, Methods for determining time of death, Forensic Sci. Med. Pathol. 12 (4) (2016) 451–485.
[20] L.A. Johnson, J.A. Ferris, Analysis of postmortem DNA degradation by single-cell gel electrophoresis, Forensic Sci. Int. 126 (1) (2002) 43–47.
[21] S. Pittner, B. Ehrenfellner, F.C. Monticelli, A. Zissler, A.M. Sanger, W. Stoiber, P. Steinbacher, Postmortem muscle protein degradation in humans as a tool for PMI delimitation, Int. J. Leg. Med. 130 (6) (2016) 1547–1555.
[22] E. Dollerup, Chemical Analyses and Microradiographic Investigations on Bone Biopsies from Cases of Osteoporosis and Osteomalacia as Compared with Normal. Part I. Calcium, Phophorus and Nitrogen Content of Normal and Osteoporotic Human Bone, Bone and Booth. The Macmillan Company, New York, NY, 1964, pp. 399–404.
[23] M. Schultz, Microscopic Investigation of Excavated Skeletal Remains: a Contribution to Paleopathology and Forensic Medicine, Forensic Taphonomy: the Postmortem Fate of Human Remains, CRC Press, Boca Raton, 1997, pp. 201–222.
[24] M. Yoshino, T. Kimijima, S. Miyasaka, H. Sato, S. Seta, Microscopical study on estimation of time since death in skeletal remains, Forensic Sci. Int. 49 (2) (1991) 143–158.
[25] A. Chibnall, M. Rees, E. Williams, The total nitrogen content of egg albumin and other proteins, Biochem. J. 37 (3) (1943) 354.
[26] F.E. Camps, J.M. Cameron, D.J. Lanham, Practical Forensic Medicine, Hutchinson, 1971.
[27] C. Cattaneo, K. Gelsthorpe, P. Phillips, R.J. Sokol, Reliable identification of human albumin in ancient bone using ELISA and monoclonal antibodies, Am. J. Phys. Anthropol. 87 (3) (1992) 365–372.
[28] N. Procopio, A. Williams, A.T. Chamberlain, M. Buckley, Forensic proteomics for the evaluation of the post-mortem decay in bones, J. Proteonomics 177 (2018) 21–30.
[29] G. Prieto-Bonete, M.D. Pérez-Cárceles, A. Maurandi-López, C. Pérez-Martínez, A. Luna, Association between protein profile and postmortem interval in human bone remains, J. Proteonomics 192 (2019) 54–63.
[30] M.A. Castellano, E.C. Villanueva, R. von Frenckel, Estimating the date of bone remains: a multivariate study, J. Forensic Sci. 29 (2) (1984) 527–534.
[31] S. Scrivano, M. Sanavio, P. Tozzo, L. Caenazzo, Analysis of RNA in the estimation of post-mortem interval: a review of current evidence, Int. J. Leg. Med. 133 (6) (2019) 1629–1640.
[32] C. Pérez-Martínez, M.D. Pérez-Cárceles, I. Legaz, G. Prieto-Bonete, A. Luna, Quantification of nitrogenous bases, DNA and Collagen type I for the estimation of the postmortem interval in bone remains, Forensic Sci. Int. 281 (2017) 106–112.
[33] E. Locci, M. Stocchero, R. Gottardo, F. De-Giorgio, R. Demontis, M. Nioi, A. Chighine, F. Tagliaro, E. d'Aloja, Comparative use of aqueous humour 1H NMR metabolomics and potassium concentration for PMI estimation in an animal model, Int. J. Leg. Med. 135 (3) (2021) 845–852.
[34] R.E. Taylor, J.M. Suchey, L.A. Payen, P.J. Slota Jr., The use of radiocarbon (14C) to identify human skeletal materials of forensic science interest, J. Forensic Sci. 34 (5) (1989) 1196–1205.
[35] A. Boaks, D. Siwek, F. Mortazavi, The temporal degradation of bone collagen: a histochemical approach, Forensic Sci. Int. 240 (2014) 104–110.

[36] F. Kanz, C. Reiter, D.U. Risser, Citrate content of bone for time since death estimation: results from burials with different physical characteristics and known PMI, J. Forensic Sci. 59 (3) (2014) 613–620.
[37] H.P. Schwarcz, K. Agur, L.M. Jantz, A new method for determination of postmortem interval: citrate content of bone, J. Forensic Sci. 55 (6) (2010) 1516–1522.
[38] V. Sterzik, T. Jung, K. Jellinghaus, M. Bohnert, Estimating the postmortem interval of human skeletal remains by analyzing their optical behavior, Int. J. Leg. Med. 130 (6) (2016) 1557–1566.
[39] B. Swift, Dating human skeletal remains:: investigating the viability of measuring the equilibrium between 210Po and 210Pb as a means of estimating the post-mortem interval, Forensic Sci. Int. 98 (1) (1998) 119–126.
[40] A. Cappella, D. Gibelli, E. Muccino, V. Scarpulla, E. Cerutti, V. Caruso, E. Sguazza, D. Mazzarelli, C. Cattaneo, The comparative performance of PMI estimation in skeletal remains by three methods (C-14, luminol test and OHI): analysis of 20 cases, Int. J. Leg. Med. 132 (4) (2018) 1215–1224.
[41] I. Szelecz, S. Lösch, C.V.W. Seppey, E. Lara, D. Singer, F. Sorge, J. Tschui, M.A. Perotti, E.A.D. Mitchell, Comparative analysis of bones, mites, soil chemistry, nematodes and soil micro-eukaryotes from a suspected homicide to estimate the post-mortem interval, Sci. Rep. 8 (1) (2018) 25.
[42] S.M. Maclaughlin-Black, R.J. Herd, K. Willson, M. Myers, I.E. West, Strontium-90 as an indicator of time since death: a pilot investigation, Forensic Sci. Int. 57 (1) (1992) 51–56.
[43] F. Introna Jr., G. Di Vella, C.P. Campobasso, Determination of postmortem interval from old skeletal remains by image analysis of luminol test results, J. Forensic Sci. 44 (3) (1999) 535–538.
[44] F. Ramsthaler, K. Kreutz, K. Zipp, M.A. Verhoff, Dating skeletal remains with luminol-chemiluminescence. Validity, intra- and interobserver error, Forensic Sci. Int. 187 (1–3) (2009) 47–50.
[45] J. Sarabia, C. Pérez-Martínez, J.P. Hernández del Rincón, A. Luna, Study of chemiluminescence measured by luminometry and its application in the estimation of postmortem interval of bone remains, Leg. Med. 33 (2018) 32–35.
[46] F. Ramsthaler, K. Kreutz, K. Zipp, M.A. Verhoff, Dating skeletal remains with luminol-chemiluminescence. Validity, intra- and interobserver error, Forensic Sci. Int. 187 (1) (2009) 47–50.
[47] F. Ramsthaler, S.C. Ebach, C.G. Birngruber, M.A. Verhoff, Postmortem interval of skeletal remains through the detection of intraosseal hemin traces. A comparison of UV-fluorescence, luminol, Hexagon-OBTI®, and Combur® tests, Forensic Sci. Int. 209 (1) (2011) 59–63.
[48] G. Piga, A. Malgosa, T. Thompson, S. Enzo, A new calibration of the XRD technique for the study of archaeological burned human remains, J. Archaeol. Sci. 35 (8) (2008) 2171–2178.
[49] M.J. Prieto-Castelló, J.P. Hernández del Rincón, C. Pérez-Sirvent, P. Álvarez-Jiménez, M.D. Pérez-Cárceles, E. Osuna, A. Luna, Application of biochemical and X-ray diffraction analyses to establish the postmortem interval, Forensic Sci. Int. 172 (2) (2007) 112–118.
[50] S. Longato, C. Woss, P. Hatzer-Grubwieser, C. Bauer, W. Parson, S.H. Unterberger, V. Kuhn, N. Pemberger, A.K. Pallua, W. Recheis, R. Lackner, R. Stalder, J. D. Pallua, Post-mortem interval estimation of human skeletal remains by micro-computed tomography, mid-infrared microscopic imaging and energy dispersive X-ray mapping, Anal. Methods 7 (7) (2015) 2917–2927.
[51] T.A. Surovell, M.C. Stiner, Standardizing infra-red measures of bone mineral crystallinity: an experimental approach, J. Archaeol. Sci. 28 (6) (2001) 633–642.
[52] T. Thompson, M. Islam, K. Piduru, A. Marcel, An investigation into the internal and external variables acting on crystallinity index using Fourier Transform Infrared Spectroscopy on unaltered and burned bone, Palaeogeogr. Palaeoclimatol. Palaeoecol. 299 (1) (2011) 168–174.
[53] S. Gourion-Arsiquaud, D. Faibish, E. Myers, L. Spevak, J. Compston, A. Hodsman, E. Shane, R.R. Recker, E.R. Boskey, A.L. Boskey, Use of FTIR spectroscopic imaging to identify parameters associated with fragility fracture, J. Bone Miner. Res. 24 (9) (2009) 1565–1571.
[54] T. Thompson, M. Gauthier, M. Islam, The application of a new method of Fourier Transform Infrared Spectroscopy to the analysis of burned bone, J. Archaeol. Sci. 36 (3) (2009) 910–914.
[55] E. Pucéat, B. Reynard, C. Lécuyer, Can crystallinity be used to determine the degree of chemical alteration of biogenic apatites? Chem. Geol. 205 (1) (2004) 83–97.
[56] Z. Patonai, G. Maasz, P. Avar, J. Schmidt, T. Lorand, I. Bajnoczky, L. Mark, Novel dating method to distinguish between forensic and archeological human skeletal remains by bone mineralization indexes, Int. J. Leg. Med. 127 (2) (2013) 529–533.
[57] G. McLaughlin, I.K. Lednev, Potential application of Raman spectroscopy for determining burial duration of skeletal remains, Anal. Bioanal. Chem. 401 (8) (2011) 2511–2518.
[58] M.A. Verhoff, K. Kreutz, E. Jopp, M. Kettner, Forensische Anthropologie im 21. Jahrhundert, Rechtsmedizin 23 (2) (2013) 79–84.
[59] G. Nagy, T. Lorand, Z. Patonai, G. Montsko, I. Bajnoczky, A. Marcsik, L. Mark, Analysis of pathological and non-pathological human skeletal remains by FT-IR spectroscopy, Forensic Sci. Int. 175 (1) (2008) 55–60.
[60] Q. Wang, Y. Zhang, H. Lin, S. Zha, R. Fang, X. Wei, S. Fan, Z. Wang, Estimation of the late postmortem interval using FTIR spectroscopy and chemometrics in human skeletal remains, Forensic Sci. Int. 281 (2017) 113–120.
[61] D. Creagh, A. Cameron, Estimating the Post-Mortem Interval of skeletonized remains: the use of Infrared spectroscopy and Raman spectro-microscopy, Radiat. Phys. Chem. 137 (2017) 225–229.
[62] C. Woess, S.H. Unterberger, C. Roider, M. Ritsch-Marte, N. Pemberger, J. Cemper-Kiesslich, P. Hatzer-Grubwieser, W. Parson, J.D. Pallua, Assessing various Infrared (IR) microscopic imaging techniques for post-mortem interval evaluation of human skeletal remains, PLoS One 12 (3) (2017) e0174552.
[63] L. Ortiz-Herrero, B. Uribe, L.H. Armas, M.L. Alonso, A. Sarmiento, J. Irurita, R.M. Alonso, M.I. Maguregui, F. Etxeberria, L. Bartolome, Estimation of the post-mortem interval of human skeletal remains using Raman spectroscopy and chemometrics, Forensic Sci. Int. 329 (2021) 111087.
[64] F. De-Giorgio, G. Ciasca, G. Fecondo, A. Mazzini, M. De Spirito, V.L. Pascali, Estimation of the time of death by measuring the variation of lateral cerebral ventricle volume and cerebrospinal fluid radiodensity using postmortem computed tomography, Int. J. Leg. Med. 135 (6) (2021) 2615–2623.
[65] L.S. Wilk, G.J. Edelman, M. Roos, M. Clerkx, I. Dijkman, J.V. Melgar, R.J. Oostra, M.C.G. Aalders, Individualised and non-contact post-mortem interval determination of human bodies using visible and thermal 3D imaging, Nat. Commun. 12 (1) (2021) 5997.
[66] J.D. Wells, M.C. Lecheta, M.O. Moura, L.R. LaMotte, An evaluation of sampling methods used to produce insect growth models for postmortem interval estimation, Int. J. Leg. Med. 129 (2) (2015) 405–410.
[67] C.-I. Chang, Hyperspectral Imaging: Techniques for Spectral Detection and Classification, Springer Science & Business Media, 2003.
[68] A. Pardo, J.A. Gutierrez-Gutierrez, I. Lihacova, J.M. Lopez-Higuera, O.M. Conde, On the spectral signature of melanoma: a non-parametric classification framework for cancer detection in hyperspectral imaging of melanocytic lesions, Biomed. Opt Express 9 (12) (2018) 6283–6301.
[69] S. Bauer, F. Puente León, Gewinnung und Verarbeitung hyperspektraler Fluoreszenzbilder zur optischen Mineralklassifikation, TM - Tech. Mess. 82 (1) (2015) 24–33.
[70] S. Bauer, F. Puente León, Spectral and geometric aspects of mineral identification by means of hyperspectral fluorescence imaging, TM - Tech. Mess. 82 (12) (2015) 597–605.
[71] J.M. Bioucas-Dias, A. Plaza, N. Dobigeon, M. Parente, Q. Du, P. Gader, J. Chanussot, Hyperspectral unmixing overview: geometrical, statistical, and sparse regression-based approaches, IEEE J. Sel. Top. Appl. Earth Obs. Rem. Sens. 5 (2) (2012) 354–379.
[72] Y.-R. Chen, K. Chao, M.S. Kim, Machine vision technology for agricultural applications, Comput. Electron. Agric. 36 (2) (2002) 173–191.
[73] J.D. Pallua, A. Brunner, B. Zelger, C.W. Huck, M. Schirmer, J. Laimer, D. Putzer, M. Thaler, B. Zelger, New perspectives of hyperspectral imaging for clinical research, NIR News 32 (3–4) (2021) 5–13.
[74] S. Turker-Kaya, C.W. Huck, A review of mid-infrared and near-infrared imaging: principles, concepts and applications in plant tissue analysis, Molecules 22 (1) (2017).
[75] C.W. Huck, Advances of vibrational spectroscopic methods in phytomics and bioanalysis, J. Pharm. Biomed. Anal. 87 (2014) 26–35.
[76] Y. Chen, C. Zou, M. Mastalerz, S. Hu, C. Gasaway, X. Tao, Applications of micro-fourier transform infrared spectroscopy (FTIR) in the geological sciences–A review, Int. J. Mol. Sci. 16 (12) (2015) 30223–30250.
[77] J.D. Pallua, A. Brunner, B. Zelger, R. Stalder, S.H. Unterberger, M. Schirmer, M.C. Tappert, Clinical infrared microscopic imaging: an overview, Pathol. Res. Pract. 214 (10) (2018) 1532–1538.

[78] C.H. Petter, N. Heigl, M. Rainer, R. Bakry, J. Pallua, G.K. Bonn, C.W. Huck, Development and application of Fourier-transform infrared chemical imaging of tumour in human tissue, Curr. Med. Chem. 16 (3) (2009) 318–326.
[79] C. Pezzei, J.D. Pallua, G. Schaefer, C. Seifarth, V. Huck-Pezzei, L.K. Bittner, H. Klocker, G. Bartsch, G.K. Bonn, C.W. Huck, Characterization of normal and malignant prostate tissue by Fourier transform infrared microspectroscopy, Mol. Biosyst. 6 (11) (2010) 2287–2295.
[80] J.D. Pallua, C. Pezzei, B. Zelger, G. Schaefer, L.K. Bittner, V.A. Huck-Pezzei, S.A. Schoenbichler, H. Hahn, A. Kloss-Brandstaetter, F. Kloss, G.K. Bonn, C. W. Huck, Fourier transform infrared imaging analysis in discrimination studies of squamous cell carcinoma, Analyst 137 (17) (2012) 3965–3974.
[81] K.B. Bec, J. Grabska, C.W. Huck, Near-infrared spectroscopy in bio-applications, Molecules 25 (12) (2020).
[82] C.W. Huck, Y. Ozaki, V.A. Huck-Pezzei, Critical review upon the role and potential of fluorescence and near-infrared imaging and absorption spectroscopy in cancer related cells, serum, saliva, urine and tissue analysis, Curr. Med. Chem. 23 (27) (2016) 3052–3077.
[83] E.J.M. Baltussen, E.N.D. Kok, S.G. Brouwer de Koning, J. Sanders, A.G.J. Aalbers, N.F.M. Kok, G.L. Beets, C.C. Flohil, S.C. Bruin, K.F.D. Kuhlmann, H. Sterenborg, T.J.M. Ruers, Hyperspectral imaging for tissue classification, a way toward smart laparoscopic colorectal surgery, J. Biomed. Opt. 24 (1) (2019) 1–9.
[84] E. Kho, L.L. de Boer, K.K. Van de Vijver, F. van Duijnhoven, M. Vrancken Peeters, H. Sterenborg, T.J.M. Ruers, Hyperspectral imaging for resection margin assessment during cancer surgery, Clin. Cancer Res. 25 (12) (2019) 3572–3580.
[85] T.J. Tsai, A. Mukundan, Y.S. Chi, Y.M. Tsao, Y.K. Wang, T.H. Chen, I.C. Wu, C.W. Huang, H.C. Wang, Intelligent identification of early esophageal cancer by band-selective hyperspectral imaging, Cancers 14 (17) (2022).
[86] T. Wagner, S. Katou, P. Wahl, F. Vogt, F. Kneifel, H. Morgul, T. Vogel, P. Houben, F. Becker, B. Struecker, A. Pascher, S. Radunz, Hyperspectral imaging for quantitative assessment of hepatic steatosis in human liver allografts, Clin. Transplant. 36 (8) (2022) e14736.
[87] H.M. Chen, Y.H. Shih, H.C. Wang, Y.H. Sun, R.C. Wang, C.J. Teng, Detection of DLBCL by pixel purity index and iterative linearly constrained minimum variance into hyperspectral imaging analysis, J. Biophot. (2022) e202200143.
[88] C. Cucci, J.K. Delaney, M. Picollo, Reflectance hyperspectral imaging for investigation of works of art: old master paintings and illuminated manuscripts, Acc. Chem. Res. 49 (10) (2016) 2070–2079.
[89] F. Lugli, G. Sciutto, P. Oliveri, C. Malegori, S. Prati, L. Gatti, S. Silvestrini, M. Romandini, E. Catelli, M. Casale, S. Talamo, P. Iacumin, S. Benazzi, R. Mazzeo, Near-infrared hyperspectral imaging (NIR-HSI) and normalized difference image (NDI) data processing: an advanced method to map collagen in archaeological bones, Talanta 226 (2021) 122126.
[90] L. Feng, B. Wu, S. Zhu, Y. He, C. Zhang, Application of visible/infrared spectroscopy and hyperspectral imaging with machine learning techniques for identifying food varieties and geographical origins, Front. Nutr. 8 (2021) 680357.
[91] F. Xing, H. Yao, Y. Liu, X. Dai, R.L. Brown, D. Bhatnagar, Recent developments and applications of hyperspectral imaging for rapid detection of mycotoxins and mycotoxigenic fungi in food products, Crit. Rev. Food Sci. Nutr. 59 (1) (2019) 173–180.
[92] H. Jiang, W. Yuan, Y. Ru, Q. Chen, J. Wang, H. Zhou, Feasibility of identifying the authenticity of fresh and cooked mutton kebabs using visible and near-infrared hyperspectral imaging, Spectrochim. Acta Mol. Biomol. Spectrosc. 282 (2022) 121689.
[93] H. Yin, B. Li, Y.D. Liu, F. Zhang, C.T. Su, A.G. Ou-Yang, Detection of early bruises on loquat using hyperspectral imaging technology coupled with band ratio and improved Otsu method, Spectrochim. Acta Mol. Biomol. Spectrosc. 283 (2022) 121775.
[94] Z. Gai, L. Sun, H. Bai, X. Li, J. Wang, S. Bai, Convolutional neural network for apple bruise detection based on hyperspectral, Spectrochim. Acta Mol. Biomol. Spectrosc. 279 (2022) 121432.
[95] L. Fu, J. Sun, S. Wang, M. Xu, K. Yao, X. Zhou, Nondestructive evaluation of Zn content in rape leaves using MSSAE and hyperspectral imaging, Spectrochim. Acta Mol. Biomol. Spectrosc. 281 (2022) 121641.
[96] J. Cheng, J. Sun, K. Yao, M. Xu, S. Wang, L. Fu, Development of multi-disturbance bagging Extreme Learning Machine method for cadmium content prediction of rape leaf using hyperspectral imaging technology, Spectrochim. Acta Mol. Biomol. Spectrosc. 279 (2022) 121479.
[97] W. Luo, G. Fan, P. Tian, W. Dong, H. Zhang, B. Zhan, Spectrum classification of citrus tissues infected by fungi and multispectral image identification of early rotten oranges, Spectrochim. Acta Mol. Biomol. Spectrosc. 279 (2022) 121412.
[98] F. Shen, H. Deng, L. Yu, F. Cai, Open-source mobile multispectral imaging system and its applications in biological sample sensing, Spectrochim. Acta Mol. Biomol. Spectrosc. 280 (2022) 121504.
[99] D.G.R.L. Books, Strafgesetzbuch von Österreich, Books on Demand, 2022.
[100] W.M. Bass, Human Osteology: a Laboratory and Field Manual of the Human Skeleton, Missouri Archaeological Society Springfield, 1971. MO.
[101] W.M. Krogman, M.Y. Iscan, The Human Skeleton in Forensic Medicine, Charles C. Thomas Springfield, 1986.
[102] C.M. Bauer, H. Niederstätter, G. McGlynn, H. Stadler, W. Parson, Comparison of morphological and molecular genetic sex-typing on mediaeval human skeletal remains, Forensic Sci. Int.: Genetics 7 (6) (2013) 581–586.
[103] G. McGlynn, Using 13C-, 15N-, and 18O Stable Isotope Analysis of Human Bone Tissue to Identify Transhumance, High Altitude Habitation and Reconstruct Palaeodiet for the Early Medieval Alpine Population at Volders, lmu, Austria, 2007.
[104] V.M. Schmidt, P. Zelger, C. Wöss, C.W. Huck, R. Arora, E. Bechtel, A. Stahl, A. Brunner, B. Zelger, M. Schirmer, W. Rabl, J.D. Pallua, Post-mortem interval of human skeletal remains estimated with handheld NIR spectrometry, Biology 11 (7) (2022).
[105] V.M. Schmidt, P. Zelger, C. Woess, A.K. Pallua, R. Arora, G. Degenhart, A. Brunner, B. Zelger, M. Schirmer, W. Rabl, J.D. Pallua, Application of micro-computed tomography for the estimation of the post-mortem interval of human skeletal remains, Biology 11 (8) (2022).
[106] A. Holmer, J. Marotz, P. Wahl, M. Dau, P.W. Kämmerer, Hyperspectral imaging in perfusion and wound diagnostics - methods and algorithms for the determination of tissue parameters, Biomed. Tech. 63 (5) (2018) 547–556.
[107] M. Fodor, L. Lanser, J. Hofmann, G. Otarashvili, M. Pühringer, B. Cardini, R. Oberhuber, T. Resch, A. Weissenbacher, M. Maglione, C. Margreiter, P. Zelger, J. D. Pallua, D. Öfner, R. Sucher, T. Hautz, S. Schneeberger, Hyperspectral imaging as a tool for viability assessment during normothermic machine perfusion of human livers: a proof of concept pilot study, Transpl. Int. : official journal of the European Society for Organ Transplantation 35 (2022) 10355.
[108] M. Fodor, P. Zelger, J.D. Pallua, C.W. Huck, J. Hofmann, G. Otarashvili, M. Pühringer, B. Zelger, M. Hermann, T. Resch, B. Cardini, R. Oberhuber, D. Öfner, R. Sucher, T. Hautz, S. Schneeberger, Prediction of Biliary Complications after Human Liver Transplantation Using Hyperspectral Imaging and Convolutional Neural Networks: A Proof-Of-Concept Study, Transplantation, 2023.
[109] M.M. Cascant, S. Rubio, G. Gallello, A. Pastor, S. Garrigues, M.d.l. Guardia, Burned bones forensic investigations employing near infrared spectroscopy, Vib. Spectrosc. 90 (2017) 21–30.
[110] G. Lu, B. Fei, Medical hyperspectral imaging: a review, J. Biomed. Opt. 19 (1) (2014) 10901.
[111] D. Ravi, H. Fabelo, G.M. Callic, G.Z. Yang, Manifold embedding and semantic segmentation for intraoperative guidance with hyperspectral brain imaging, IEEE Trans Med Imaging 36 (9) (2017) 1845–1857.
[112] A. Pardo, E. Real, V. Krishnaswamy, J.M. Lopez-Higuera, B.W. Pogue, O.M. Conde, Directional kernel density estimation for classification of breast tissue spectra, IEEE Trans Med Imaging 36 (1) (2017) 64–73.
[113] M. Milanic, L.A. Paluchowski, L.L. Randeberg, Hyperspectral imaging for detection of arthritis: feasibility and prospects, J. Biomed. Opt. 20 (9) (2015) 096011.
[114] S.V. Panasyuk, S. Yang, D.V. Faller, D. Ngo, R.A. Lew, J.E. Freeman, A.E. Rogers, Medical hyperspectral imaging to facilitate residual tumor identification during surgery, Cancer Biol. Ther. 6 (3) (2007) 439–446.
[115] M.E. Martin, M.B. Wabuyele, K. Chen, P. Kasili, M. Panjehpour, M. Phan, B. Overholt, G. Cunningham, D. Wilson, R.C. Denovo, T. Vo-Dinh, Development of an advanced hyperspectral imaging (HSI) system with applications for cancer detection, Ann. Biomed. Eng. 34 (6) (2006) 1061–1068.
[116] J. Laimer, E. Bruckmoser, T. Helten, B. Kofler, B. Zelger, A. Brunner, B. Zelger, C.W. Huck, M. Tappert, D. Rogge, M. Schirmer, J.D. Pallua, Hyperspectral imaging as a diagnostic tool to differentiate between amalgam tattoos and other dark pigmented intraoral lesions, J. Biophot. (2020) e202000424.
[117] E. Willenbacher, A. Brunner, W. Willenbacher, B. Zelger, D. Wolf, D. Rogge, M. Tappert, J.D. Pallua, Visible and near-infrared hyperspectral imaging techniques allow the reliable quantification of prognostic markers in lymphomas: a pilot study using the Ki67 proliferation index as an example, Exp. Hematol. 91 (2020).

[118] P. Liu, J. Huang, S. Zhang, R.X. Xu, Multiview hyperspectral topography of tissue structural and functional characteristics, J. Biomed. Opt. 21 (1) (2016) 16012.
[119] H.T. Lim, V.M. Murukeshan, A four-dimensional snapshot hyperspectral video-endoscope for bio-imaging applications, Sci. Rep. 6 (2016) 24044.
[120] S.J. Leavesley, M. Walters, C. Lopez, T. Baker, P.F. Favreau, T.C. Rich, P.F. Rider, C.W. Boudreaux, Hyperspectral imaging fluorescence excitation scanning for colon cancer detection, J. Biomed. Opt. 21 (10) (2016) 104003.
[121] R.T. Kester, N. Bedard, L. Gao, T.S. Tkaczyk, Real-time snapshot hyperspectral imaging endoscope, J. Biomed. Opt. 16 (5) (2011) 056005.
[122] L. Gao, R.T. Smith, Optical hyperspectral imaging in microscopy and spectroscopy - a review of data acquisition, J. Biophot. 8 (6) (2015) 441–456.
[123] F. Blanco, F. Lumbreras, J. Serrat, R. Siener, S. Serranti, G. Bonifazi, M. Lopez-Mesas, M. Valiente, Taking advantage of hyperspectral imaging classification of urinary stones against conventional infrared spectroscopy, J. Biomed. Opt. 19 (12) (2014) 126004.
[124] S. Ortega, M. Halicek, H. Fabelo, G.M. Callico, B. Fei, Hyperspectral and multispectral imaging in digital and computational pathology: a systematic review [Invited], Biomed. Opt Express 11 (6) (2020) 3195–3233.
[125] B. Regeling, B. Thies, A.O. Gerstner, S. Westermann, N.A. Muller, J. Bendix, W. Laffers, Hyperspectral imaging using flexible endoscopy for laryngeal cancer detection, Sensors 16 (8) (2016).
[126] Z. Han, A. Zhang, X. Wang, Z. Sun, M.D. Wang, T. Xie, In vivo use of hyperspectral imaging to develop a noncontact endoscopic diagnosis support system for malignant colorectal tumors, J. Biomed. Opt. 21 (1) (2016) 16001.
[127] R. Koprowski, S. Wilczynski, Z. Wrobel, B. Blonska-Fajfrowska, Calibration and segmentation of skin areas in hyperspectral imaging for the needs of dermatology, Biomed. Eng. Online 13 (2014) 113.
[128] G. Lu, J.V. Little, X. Wang, H. Zhang, M.R. Patel, C.C. Griffith, M.W. El-Deiry, A.Y. Chen, B. Fei, Detection of head and neck cancer in surgical specimens using quantitative hyperspectral imaging, Clin. Cancer Res. 23 (18) (2017) 5426–5436.
[129] M. Halicek, H. Fabelo, S. Ortega, J.V. Little, X. Wang, A.Y. Chen, G.M. Callico, L. Myers, B.D. Sumer, B. Fei, Hyperspectral imaging for head and neck cancer detection: specular glare and variance of the tumor margin in surgical specimens, J. Med. Imaging 6 (3) (2019) 035004.
[130] B. Kim, N. Kehtarnavaz, P. LeBoulluec, H. Liu, Y. Peng, D. Euhus, Automation of ROI extraction in hyperspectral breast images, Annu Int Conf IEEE Eng Med Biol Soc 2013 (2013) 3658–3661.
[131] M. Halicek, M. Shahedi, J.V. Little, A.Y. Chen, L.L. Myers, B.D. Sumer, B. Fei, Head and neck cancer detection in digitized whole-slide histology using convolutional neural networks, Sci. Rep. 9 (1) (2019) 14043.
[132] A. Brunner, E. Willenbacher, W. Willenbacher, B. Zelger, P. Zelger, C.W. Huck, J.D. Pallua, Visible- and near-infrared hyperspectral imaging for the quantitative analysis of PD-L1+ cells in human lymphomas: comparison with fluorescent multiplex immunohistochemistry, Spectrochim. Acta Mol. Biomol. Spectrosc. 285 (2023) 121940.
[133] A. Brunner, V.M. Schmidt, B. Zelger, C. Woess, R. Arora, P. Zelger, C.W. Huck, J. Pallua, Visible and Near-Infrared hyperspectral imaging (HSI) can reliably quantify CD3 and CD45 positive inflammatory cells in myocarditis: pilot study on formalin-fixed paraffin-embedded specimens from myocard obtained during autopsy, Spectrochim. Acta Mol. Biomol. Spectrosc. 274 (2022) 121092.